Journal of Materials Chemistry A

Accepted Manuscript

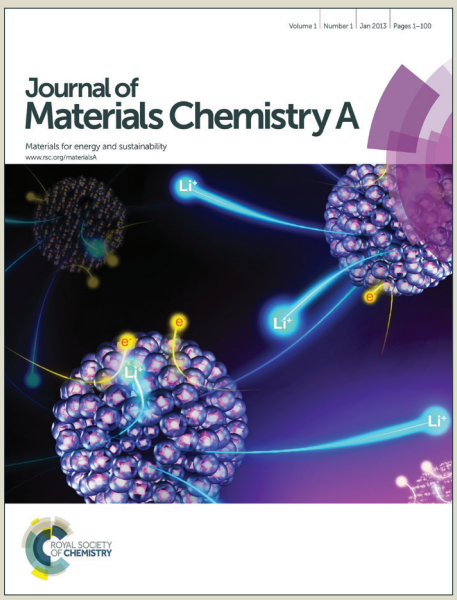

This is an *Accepted Manuscript*, which has been through the Royal Society of Chemistry peer review process and has been accepted for publication.

Accepted Manuscripts are published online shortly after acceptance, before technical editing, formatting and proof reading. Using this free service, authors can make their results available to the community, in citable form, before we publish the edited article. We will replace this *Accepted Manuscript* with the edited and formatted *Advance Article* as soon as it is available.

You can find more information about *Accepted Manuscripts* in the Information for Authors.

Please note that technical editing may introduce minor changes to the text and/or graphics, which may alter content. The journal's standard Terms & Conditions and the Ethical guidelines still apply. In no event shall the Royal Society of Chemistry be held responsible for any errors or omissions in this *Accepted Manuscript* or any consequences arising from the use of any information it contains.

ROYAL SOCIETY OF CHEMISTRY

www.rsc.org/materialsA

Cite this: DOI: 10.1039/c0xx00000x

www.rsc.org/xxxxxx

ARTICLE TYPE

Graphene fiber-based asymmetric micro-supercapacitors

Bingna Zheng [a], Tieqi Huang [a], Liang Kou [a], Xiaoli Zhao [a], Karthikeyan Gopalsamy [a], Chao Gao*[a]

Received (in XXX, XXX) Xth XXXXXXXXX 20XX, Accepted Xth XXXXXXXXX 20XX
DOI: 10.1039/b000000x

Fiber-based micro-supercapacitors (F-mSCs) are new members of the energy storage family, which facilitate SCs with flexibility and expand their application to fields such as tiny, flexible and wearable devices. One of the biggest challenges for F-SCs is to enhance the energy density (*E*) and keep the flexibility at the same time. Here, for the first time we assembled a kind of fiber-based asymmetric micro-supercapacitors (F-*asym*-mSCs) with two different graphene fiber-based electrodes. The excellent electrochemical performances (59.2 mF/cm^2 and 32.6 mF/cm^2, respectively) of both electrodes offered a chance to achieve high performance two-ply F-*asym*-mSCs. The potential window of F-*asym*-mSCs was expanded to 1.6 V, and both of the area energy density (E_A , 11.9 μWh/cm^2) and volume energy density (E_V, 11.9 mWh/cm^3) are the highest *E* ever reported in F-SCs. The F-*asym*-mSCs exhibit good cycling stability with a 92.7% initial capacitance retention after 8000 cycles and can be integrate into a fiber-like device to realize the flexibility of fibers.

Introduction

Supercapacitors (SCs), also known as electro-chemical capacitors, are widely used in many fields such as hybrid electric vehicles and memory back-up devices because of the high power density, fast charge-discharge rate and long cycling life. [1, 2] To meet the fast growing energy demands of human life, light-weight, flexible and portable devices with high power (*P*) and energy density (*E*) are new targets in nowadays energy storage research field.

One approach to fulfill the above targets is to assemble hybrid SCs which integrated the excellent cycling stability of carbon materials [3-7] with the high specific capacitance of metal oxides [8-11] and conducting polymers [12-14] together. Apart from optimizing the electrode materials of symmetric supercapacitors (*sym*-SCs), asymmetric supercapacitors (*asym*-SCs) have been an upgrade version of hybrid SCs because they can improve the energy density by expanding operating voltage window in aqueous electrolyte. [51] Even though conventional button *asym*-SCs [15, 16] and flexible paper *asym*-SCs [17-21] have been widely recognized, fiber-based *asym*-SCs (F-*asym*-SCs) have never been reported to our knowledge likely due to the difficulty of accessing different, compatible fiber electrodes.

Fiber-based micro-supercapacitors (F-mSCs) are new members of SCs family and have attracted increasing attention of researchers because of their flexibility and weavability. The main challenge of F-mSCs is to significantly improve their *E* while keeping relatively high *P*. Intensive efforts have been devoted to improve the area energy density (E_A) of F-SCs from 0.027 to 9.8 μWh/cm^2 by increasing the specific capacity (*C*) [12, 22-31, 52]. Since every material has its theoretical maximum *C*, such a methodology is limited to highly improve *E* of F-mSCs for a specific system. Alternatively, we consider to improve *E* of F-SCs by enlarging their operating voltage window ($E = 1/2CV^2$) *via* construction of asymmetric F-mSCs (F-*asym*-mSCs). Considering the high conductivity, high mechanical strength, outstanding flexibility and light weight of graphene fibers [32-38, 52, 57], here for the first time we developed a novel kind of flexible two-ply F-*asym*-mSCs device assembled by MnO_2-coated core-sheath graphene fiber (GMF) and graphene-carbon nanotubes hybrid fiber (GCF) in PVA/ LiCl gel electrolyte. Our F-*asym*-mSCs showed E_A up to 11.9 μWh/cm^2 (or volume energy density, E_V 11.9 mWh/cm^3), the highest value for F-mSCs. The F-*asym*-mSCs expand the vision for performance improvement of F-SCs and offer great chance for light-weight, flexible and high energy density storage devices.

Results and discussion

To assemble the F-*asym*-mSCs, we firstly made the different fiber electrodes of GMF and GCF. GMF was obtained by depositing flower-like MnO_2 nanocrystal sheath on graphene fiber (GF). The GFs were fabricated by wet-spinning of graphene oxide liquid crystal dispersion into a Mn^{2+}-contained coagulation bath, followed by chemical reduction. [32-34] After immersing GFs in a potassium permanganate ($KMnO_4$) solution for given time (1-24 h), GMFs with controlled thickness of MnO_2 sheath were achieved. With different reaction time (1, 5, 9, 12 and 24 h), GMFs are named GMF1, GMF5, GMF9, GMF12 and GMF24, respectively. The GMFs showed good mechanical strength and flexibility (Figure S1).

Journal of Materials Chemistry A Accepted Manuscript

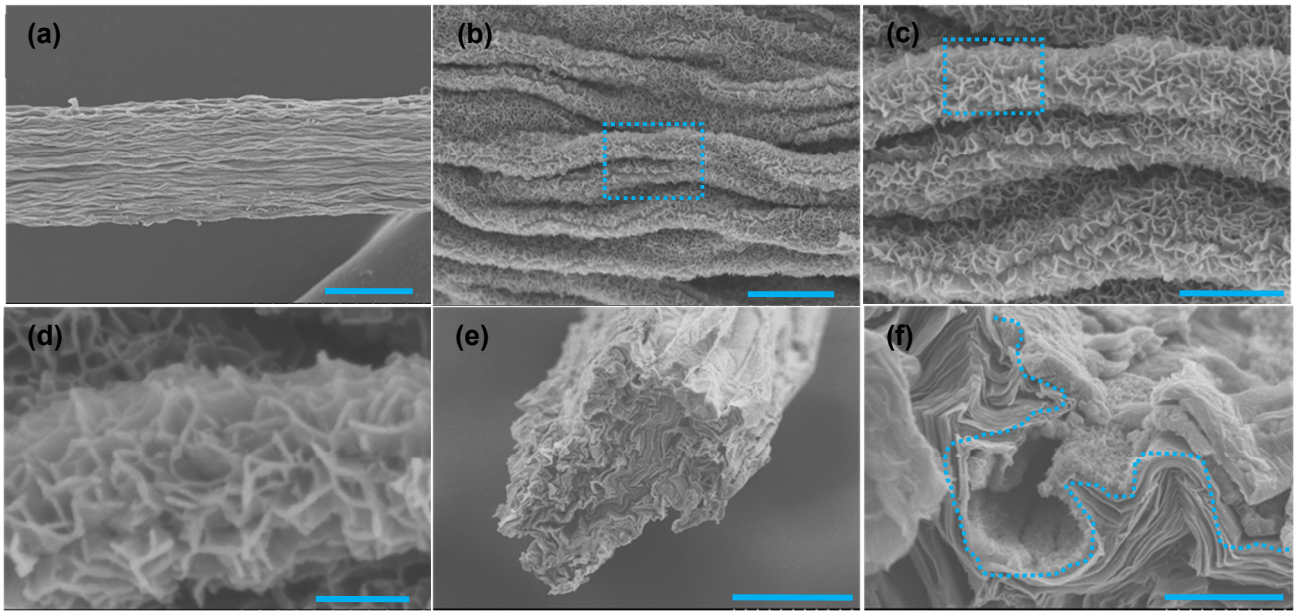

Figure 1. (a) - (d) Surface morphology of GMF1 observed by SEM, scale bar: 10 μm, 1 μm, 500 nm, and 150 nm. (e) and (f) Cross-section images of GMF1 observed by SEM, scale bar: 10 μm and 1 μm.

Reactions between Mn^{2+}, carbon and $KMnO_4$ led to the formation of MnO_2 (Equation 1 and 2) [40].

$$2MnO_4^- + 3Mn^{2+} + 2H_2O \text{ —— } 5MnO_2 + 4H^+ \quad (1)$$

$$4MnO_4^- + 3C + H_2O \text{ —— } 4MnO_2 + CO_3^{2-} + 2HCO_3^- \quad (2)$$

Flower-like MnO_2 nanocrystals were evenly distributed on the surface of GMFs, resulting in a core-sheath morphology as seen in SEM images (Figure 1a-f). The surfaces of both graphene fibers (Figure S2a) and GMFs (Figure 1a) showed many continuous wrinkles along the fibers axis, which were caused by the shrinking of graphene sheets during the drying procedure in the wet-spinning process. The wrinkles enhance the surface area of fibers and create more room for the stable growth of MnO_2 nanocrystals. Under the magnified image (Figure 1b-1d, S2d, 2f and 2h), compared with the clean surface of GFs (Figure S2b), vivid flower-like nanoribbons are uniformly distributed on GMF surface, giving rise to core-sheath structure (Figure 1e,f).

Figure 2a-d showed the energy-dispersive spectroscopy (EDS) mapping of the cross-section for GMF24, demonstrating the existence of C, O and Mn elements. The distributions of C and Mn make perfect complementary with each other, confirming the core-sheath morphorlogy. The thickness of MnO_2 sheath increased upon the reaction time, and the maximum thickness is about 1 μm (GMF24, Figure S2i- 2k).[41] Some cleavages exist on the fiber with the increase of MnO_2 sheath thinkness (Figure S2c, 2e, 2g). The cleavages have dual influence on the fibers. On the one hand, more ions could insert into the electrode system which may contribute to the fast charge/ discharge process. On the other hand, cleavages may bring about the separation and exfoliation of MnO_2 sheath from the GF surface which may reduce the amount of electrochemical active materials and cause decrease in capacitance. The fracture tip of GMF was also observed by transmission electron microscope (TEM), as shown in Figure S2l. The dragged out graphene sheets were clearly observed. Inside the dashed box, typical MnO_2 nano-structures were found around the fiber.

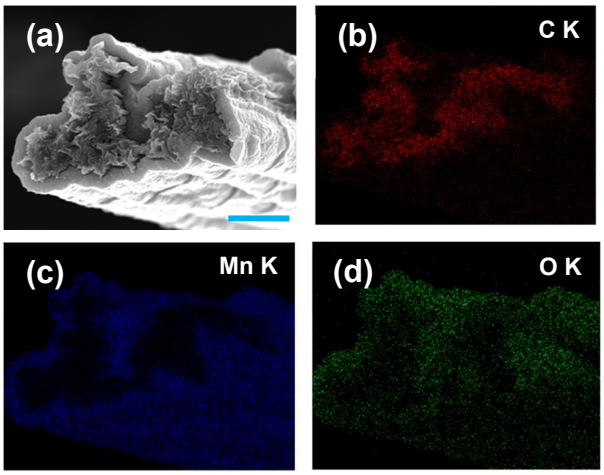

Figure 2. (a) - (d) Elemental mapping images of GMF24 by EDAX, scale bar: 10 μm

Figure 3a shows the X-ray diffraction (XRD) patterns of GMFs with different reaction time. The peak at around 24° corresponds to the (002) plane of carbon (stacked graphene sheets, d space = 0.37 nm). According to the PDF card (no. 30-820) of □-MnO_2, peaks at around 37° and 67° correspond to the (100) and (110) planes of MnO_2, respectively.[42] With the increase of sheath thickness, the characteristic peaks of MnO_2 become more intensive. The □-MnO_2 structure was also verified by the typical peaks at wavenumbers of 575 cm^{-1} and 649 cm^{-1} in corresponding Raman spectra (Figure 3b).[20]

X-ray photoelectron spectroscopy (XPS) was used to further analyze the compositions of GMF (Figure 3c-e). In Figure 3c, the peaks at 284.8 eV (C-C/C=C bonds), 286.5eV (C-O bonds), 287.6 eV (C=O bonds), and 288.8 eV (C(=O)-O bonds) indicate the chemically reduced graphene structures with strong C-C/C=C bonds. [43] Figure 3d showed the O_{1s} peaks at 529.9 eV (C=O, C(=O)-O or Mn-O) and 533 eV (C-OH).[15] In Figure 3e, two strong peaks are clearly observed at 642.6 eV and 653.9 eV, which can be asigned to the binding energy values of Mn $2p_{3/2}$

Journal of Materials Chemistry A Accepted Manuscript

This journal is © The Royal Society of Chemistry [year]

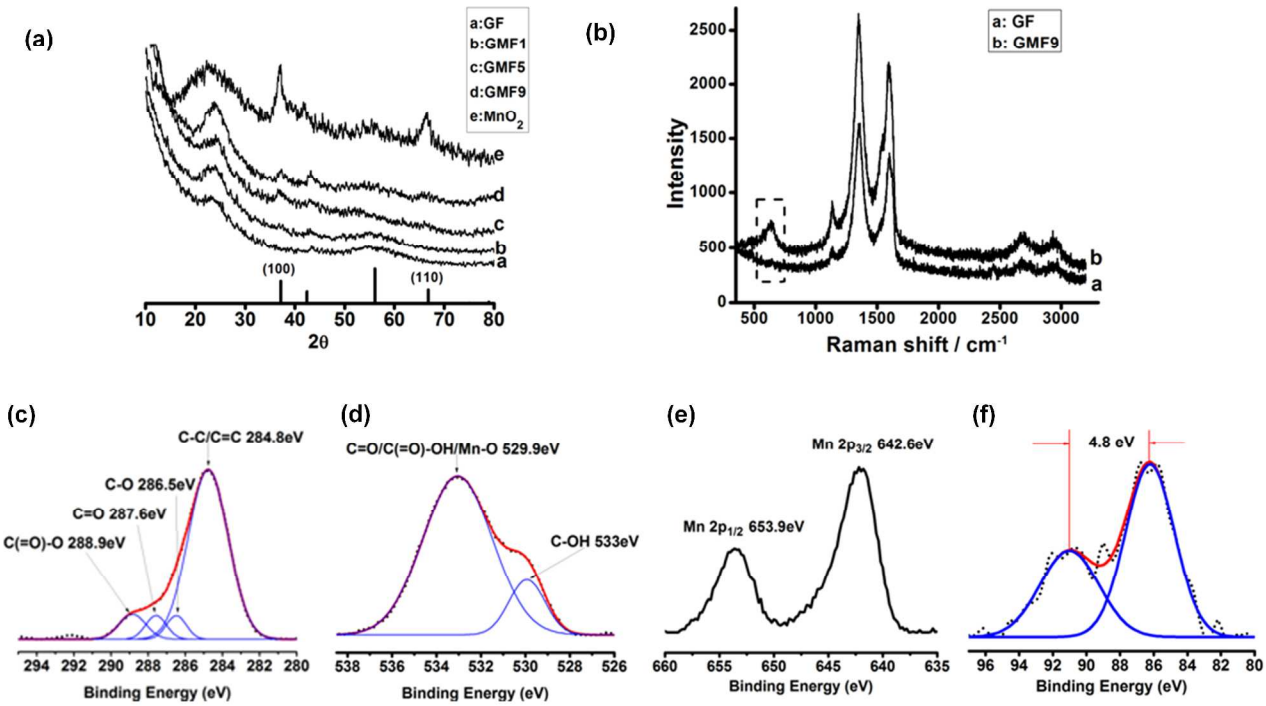

Figure 3. (a) XRD spectra of neat GF, GMF1, GMF5, GMF9, and MnO_2 comparing with standard XRD peak of ε -MnO_2. (b) Raman spectra of neat GF and GMF9. (c), (d), (e) and (f) C_{1s}, O_{1s}, Mn_{2p} and Mn_{3s} peaks in XPS of GMF, respectively.

and Mn $2p_{1/2}$, respectively. [18] The multiplet splitting which will result the separation of peak energies (Δ E) of Mn_{3s} peaks according to literature,[59] and Δ E of MnO, Mn_3O_4, Mn_2O_3 and MnO_2 are 5.79, 5.50, 5.41 and 4.78 eV, respectively. The Δ E of GMF9 is 4.8 eV as shown in Figure 3f, indicating the sheath of GMF9 is MnO_2.

The flexible GMFs were assembled into F-mSCs as illustrated in Figure 4a: two GMFs were fixed by current collector of silver paint and immersed in aqueous electrolyte (1 M Na_2SO_4). The electrochemical performance of GMFs was initially measured by cyclic voltammetry (CV). As shown in Figure 4a, CV curves of GMF9 are all parallelogram-like shaped which means a continuous, fast and reversible redox reaction took place around the surface of GMFs.[18] The integral area of GMFs with different reaction time increased firstly and decreased after 9 h (Figure 4b). Similar tendencies were also observed in corresponding galvanostatic charge-discharge (GCD) curves (Figure 4c). The area specific capacitances for single electrode (C_A) calculated from CV curves for different samples were shown in Figure S5. The C_A at a 10 mV/s scanning rate increased from 11.7 mF/cm^2 for neat GFs to 55.0 mF/cm^2 for GMF9 due to the coating of MnO_2 nanocrystals, and then decreased to 31.4 mF/cm^2 for GMF12 likely owing to the inefficient charge transportation caused by the thick sheath. [41] The highest C_A associated with GMF9 is 55 mF/cm^2, which is ~5 times of neat GF (11.7 mF/cm^2), and also much higher than those of previous graphene-based F-mSCs [28, 29, 48, 52]. C_A of GMF9 calculated by GCD is 59.2 mF/cm^2 at a current density of 0.1 mA/cm^2, also around 5 times of neat GF (12.6 mF/cm^2). According to the length and diameter of GMF9, the volume specific capacitance (C_V) of 169 F/cm^3 and linear specific capacitance (C_L) of 0.026 F/m were calculated (see calculation in the Supporting information). The E_As have also been improved dramatically from 0.27 μWh/cm^2 for GFs to 1.2 μWh/cm^2 for GMF9. E_A (1.2 μWh/cm^2) and E_V (3.4 mWh/ cm^3) for GMF9 have also exceeded the majority of values reported for F-SCs [26, 28, 30, 46-47, 49-50] and at the same orders of magnitudes of

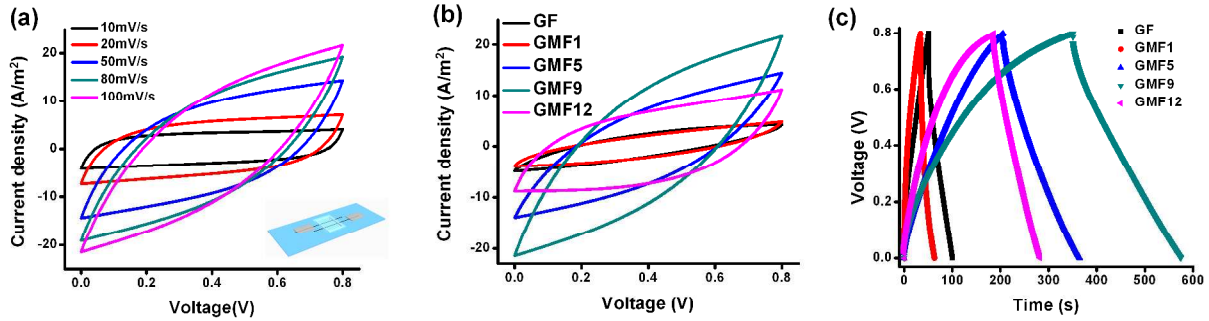

Figure 4. (a) CV curves of GMF9 at different scan rates, inset: cartoon illustration of F-mSC. (b) CV curves of neat GF, GMF1, GMF5, GMF9, and GMF12 at 100 mV/s. (c) GCD curves of neat GF, GMF1, GMF5, GMF9, and GMF12 at current density of 0.1 mA/cm^2.

Journal of Materials Chemistry A Accepted Manuscript

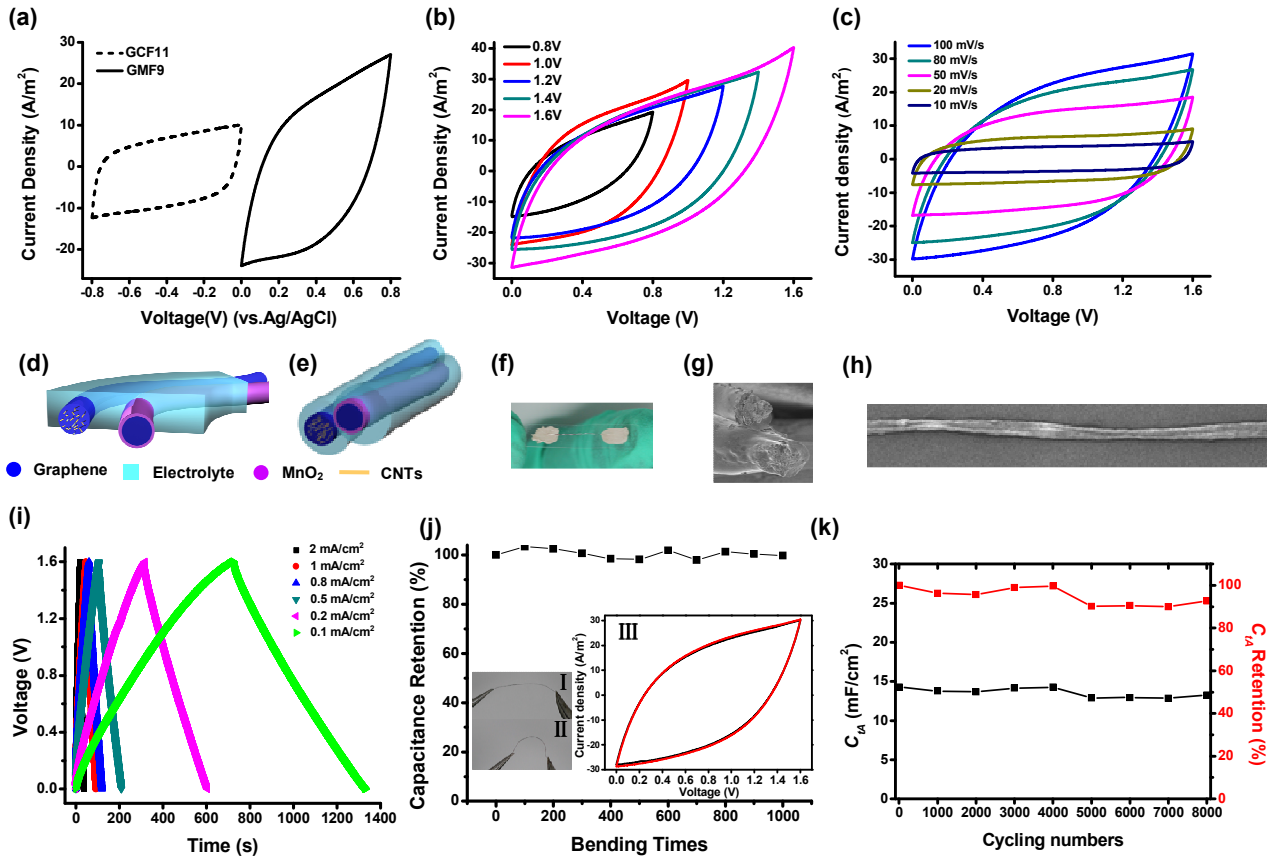

Figure 5. (a) CV curves of GMF and GCF in three-electrode system (vs. Ag/AgCl). (b) CV curves of parallel F-*asym*-mSCs at different potential windows (scanning rate 100 mV/s). (c) CV curves of two-ply F-*asym*-mSC at different scanning rates when operating voltage is 1.6 V. (d) Cartoon illustration of parallel F-*asym*-mSCs. (e) Cartoon illustration of two-ply F-*asym*-mSC. (f) Photograph of two-ply F-*asym*-mSC. (g) Cross-section image of two-ply F-*asym*-mSC observed by SEM, scale bar: 100 μm. (h) Surface image of two-ply F-*asym*-mSC observed by SEM, scale bar: 500 μm. (i) GCD curves of two-ply F-*asym*-mSC at different current densities when operating voltage is 1.6 V. (j) Capacitance retention at different bending times, inset: photos of two-ply F-*asym*-mSC at flat (i) and bending (ii) states, (iii) CV curves of two-ply F-*asym*-mSC at flat and bending states (scanning rate 100 mV/s). (k) Cycling performance of two-ply F-*asym*-mSCs tested by GCD at 1.0 mA/cm^2.

F-SCs constructed by CNT- MnO_2 [22], CNT-OMC [25] and pen ink [31]. Cyclic stability of GMF9 was conducted by GCD tests between 0 and 0.8 V at a current density of 0.1 mA/cm^2 (Figure 4d). After 1000 charge-discharge cycles, GMF9 showed good stability and still retained 95.7% of the initial specific capacitance (Figure S3).

Another electrode we used to construct F-*asym*-mSCs was GCF. The synergistic effect between graphene and carbon nanotubes (CNTs) has been recognized in aerogels and flat SCs[3, 44, 45, 60], but rarely reported in F-SCs [54- 56]. Here, multiwalled CNTs (MWNTs) were evenly dispersed in the GO liquid crystal aqueous solution (GO/MWNT = 1:1 by weight) and assembled into continuous macroscopic fibers by wet-spinning method. The typical accordion-like wrinkles still exist on the cross-section of GCFs and hairy MWNTs were dragged out from graphene sheets (Figure S4a-b). After chemical reduction by HI, GCFs are ideal candidates for electrical double-layer supercapacitors because the sandwich-like structure not only guarantees good electric conductivity but also provides channels for efficient ion transportation. In CV tests, charge/discharge loop of GCF (Figure S4c) at different scanning rates showed rectangle-like shapes which prove the electrical double-layer behavior of GCFs. C_A calculated from CV curves of GCF reached 29 mF/cm^2 at a scanning rate of 10 mV/s. The GCD curves of GCFs at different current density were shown in Figure S4d. C_A calculated from GCD curves reached 32.6 mF/cm^2 at 0.1 mA/cm^2, which is about 3 times of GFs. E_A (1.1 μWh/cm^2) and E_V (1.0 mWh/ cm^3) for GCF have also been improved comparing with other neat graphene F-SCs.

The performances of GMFs and GCFs were summarized in Table 1 and Figure S4. Both GMFs and GCFs are superior to the neat GFs, offering a chance to assemble high performance F-*asym*-mSCs. Due to the light weight of fibers, it is hard to give the exact weight of active materials of both electrodes. So we chose GMF9 and GCF with the same diameter (40 μm) by controlling the wet-spinning parameters to construct F-*asym*-mSCs, which means the surface areas of both electrodes were nearly the same. According to CV curves tested by three-electrode system (Figure 5a), GMF and GCF have stable potential windows between 0 -0.8 V and -0.8-0 V (vs. Ag/AgCl), respectively. Hence, the operating voltage was extended to 1.6 V when GMF and GCF were assembled into parallel-type F-*asym*-mSCs. GMF was assembled as positive electrode and GCF was negative electrode (Figure 5d). Figure 5b shows CV curves of different operating voltages at 100 mV/s for the parallel-type F-*asym*-mSCs. When tested by GCD at 0.5 mA/cm^2 with different voltage windows ranging from 0.8 V to 1.6 V (Figure S6a), the area capacitances of the total cell (C_{tA}) were 14.9, 14.1, 18.1,

This journal is © The Royal Society of Chemistry [year]

Journal of Materials Chemistry A Accepted Manuscript

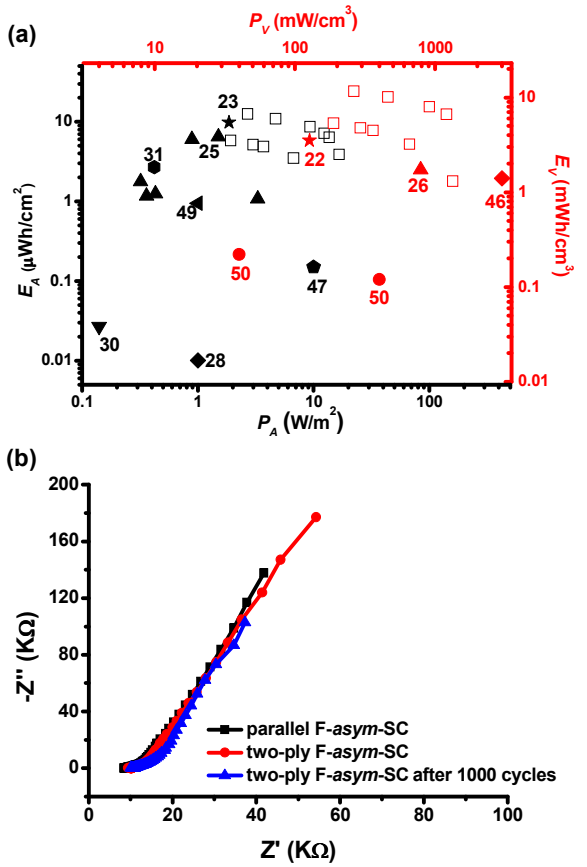

Figure 6. (a) E_A-P_A and E_V-P_V plots of F-*asym*-mSCs and references, where the black symbols are calculated by area and red symbols are calculated by volume, square symbols are data of this work. (b) Nyquist plots of F-*asym*-mSCs.

18.9, and 23.6 mF/cm^2, respectively. The highest C_{tA} can also be converted to specific volume capacitance (C_{tV}) and specific linear capacitance (C_{tL}), which were 23.6 F/cm^3 and 0.3 mF/cm, respectively. Correspondingly, the E_A also increased significantly from 1.2, 1.8, 3.4, 4.9, to 8.0 μWh/cm^2 when P_As were 0.9, 1.2, 1.5, 1.7 to 1.9 W/m^2. However, due to the imperfection device design of parallel-type F-*asym*-mSCs, current leakage happened when electrochemical reactions took place (Figure S6). To develop a new type of F-*asym*-mSC which can avoid current leakage while realize the good flexibility is essential. According to the literature[12, 58], two-ply FSCs integrated by two fiber electrodes closely are helpful. Accordingly, we also made two-ply F-*asym*-mSCs with the different electrodes of GMF and GCF, using PVA/LiCl gel as electrolyte (Figure 5e). [21] The two fiber electrodes were glued by PVA/LiCl gel after they were covered by pure PVA gel as shown in Figure 5f-h.

Figure 5c and 5i show the performances of two-ply F-*asym*-mSCs at different scanning rates and current densities when operating voltage is 1.6 V in CV and GCD tests. The C_{tA} of F-*asym*-mSCs were 33.6 mF/cm^2 and 19.1 mF/cm^2 as tested by CV at 10 mV/s and by GCD at 0.1 mA/cm^2.Values of C_{tA} and E_A in CV and GCD are also shown in Table S1-S2 and Figure S7. Furthermore, the two-ply F-*asym*-mSCs showed almost overlapped CV curves at flat and bending states (Figure 5j), confirming their good flexibility which indicates potential application in practical flexible devices. Cycling stability tests of two-ply F-*asym*-mSCs was conducted at high current density of 1.0 mA/cm^2 (Figure 5k) and 92.7% initial capacitance were retained after 8000 cycles.

In CV tests, energy densities increased from 6.1 μWh/cm^2 (6.1 mWh/cm^3) at 100 mV/s to 11.9 μWh/cm^2 (11.9 mWh/cm^3) at 10 mV/s. In GCD measurements, energy densities increased from 3.2 μWh/cm^2 (3.2 mWh/cm^3) at 2.0 mA/cm^2 to 6.7 μWh/cm^2 (6.7 mWh/cm^3) at 0.1 mA/cm^2. Figure 6a shows clear *P*-*E* comparison plots of our work and literatures. Notably, the energy density obtained from both CV and GCD tests for two-ply F-*asym*-mSCs are the highest values ever reported for F-SCs to our knowledge (Table 1), which obviously exceeded the published highest E_A (9.8 μWh/cm^2) [23] and E_V (3.5 mWh/cm^3) [22] . Moreover, our F-*asym*-mSCs dramatically increased the *E* of graphene-based F-mSCs about 70 times from 0.17μWh/cm^2 to 11.7μWh/cm^2.[28]

Electrochemical impedance spectroscopy (EIS) was carried out over the frequency range from 10^{-2}- 10^6 Hz as shown in Figure 6b. The intercepts at x axis and slopes for F-*asym*-mSCs shown in Nyquist plots mean the equivelant series resistance (ESR) and charge transport resistance in parallel F-*asym*-mSCs are smaller than that in two-ply F-*asym*-mSCs. The above phenomena explain the slight differences of electrochemical performances in the parallel and two-ply F-*asym*-mSCs. After 1000 cyclings, the ESR showed no significant changes of the equivelant resistances (~10 KΩ) which indicates the stable electrochemical performance of two-ply F-*asym*-mSCs in cycling test. The large equivelant resistances were likely caused by the large distance between two fibers and the contact resistance at current collectors. How to reduce the ESR of device is the next target of our F-*asym*-mSCs and works reported by other groups may offer some inspirations.[23, 25]

Experimental

Preparation of GMFs

Graphene fibers were prepared by injecting liquid-crystal graphene oxide (GO) into a rotating coagulation bath of 5 wt% manganese acetate ($Mn(Ac)_2$) in ethanol/water (volume ratio 1:3). After being immersed in coagulation bath for 15 min, the gel-like fibers were taken out and immersed in ethanol/water solution for 0.5 h. Then the graphene oxide fibers were dried at 90 °C in vacuum oven over night and reduced by diluted hydroiodic acid (HI) at 90 °C for 1 h. The GFs were then immersed in 0.05wt% $KMnO_4$ solution with given reaction time and then washed by water. After drying at 90°C over night, GMFs were obtained.

Preparation of GCFs

Dispersible MWNTs were prepared according to the reported protocol. [53] MWNTs were mixed with GO (1:1 by weight) liquid crystal aqueous solution and vigorously stirred for 1 h at room temperature. The mixtures were injected into rotating coagulation bath of $CaCl_2$ in ethanol/water (volume ratio 1:3). After immersed for 15 min, fibers were taken out and washed by ethanol/water solution for 0.5 h. Then the GO/CNTs fibers were dried at 90 °C in vacuum oven over night and reduced by diluted hydroiodic acid (HI) at 90 °C for 1 h. After washing with ethanol and drying at room temperature, GCFs were obtained.

Journal of Materials Chemistry A Accepted Manuscript

Fabrication of F-mSCs

Two fiber electrodes with the same diameter were fixed at two ends by silver paint. 1 M Na_2SO_4 solution was sealed into the cell constructed by PET film and glass cement, affording parallel F-*sym*-mSCs or F-*asym*-mSCs. For two-ply F-*asym*-mSCs, fiber electrodes were firstly covered by pure PVA solution and dried under infrared lamp and then glued by PVA/LiCl gel electrolyte as previously reported. [21] The two ends of electrodes were fixed at PET film by silver paint.

Characterizations

SEM images were taken on a Hitachi S3000N field-emission SEM; TEM images were taken on a JEM-1200EX; XRD data were collected with a X'Pert PRO (PANalytical) diffractometer using monochromatic Cu Kα1 radiation (λ= 1.5406 Å) at 40 kV; Raman measurements were conducted on inVia-Reflex; XPS measurements were conducted on a PHI 5000C ESCA system operated at 14.0 KV and all the binding energies were referenced to the C1S neutral carbon peak at 284.8 eV; CV, GCD and EIS measurments were conducted by a CHI660E workstation (CH Instruments, Inc.).

Conclusion

In summary, we have prepared two different graphene-based fiber electrodes based on the facile wet-spinning assembly method. The core-sheath GMFs integrated the advantages of pseudo-capacitance of MnO_2 and conductivity of graphene. The C_A of GMFs reached 59.2 mF/cm^2, five times that of the neat GFs. The synergistic effect of graphene and CNTs enhanced C_A of GCFs to 32.6 mF/cm^2. For the first time, we fabricated asymmetric fiber-based supercapacitors, F-*asym*-SCs, from the excellent GMF and GCF electrodes. The capacitance of whole cell achieved (C_{tA}) up to 23.6 mF/cm^2 when the operating voltage window was increased to 1.6 V. Due to the large voltage window, the energy densities of flexible F-*asym*-SCs were significantly improved to 11.9 μWh/cm^2, the highest values ever reported for all F-SCs. The F-*asym*-SCs exhibit good cycling stability with a 96.3% initial capacitance retention after 1000 cycles. Our approach opened a new avenue to design and fabricate high performance yarn supercapacitors, and paves the way to high energy density, wearable electronic devices [61, 62].

Table 1. Capacitance and energy density comparison of F-mSCs.

Ref	Electrode Materials	*C*			*E*	
		C_A (mF/cm^2)	C_V (F/cm^3)	C_L (mF/cm)	E_A (μWh/cm^2)	E_V (mWh/cm^3)
This work	GMF9	59.2	169.0	0.33	1.2	3.4
	GCF	32.6	29.1	0.46	1.1	1.0
	Two-ply F-*asym*-mSC[a]	**33.6***	**33.6***	**0.42***	**11.9**	**11.9**
	Two-ply F-*asym*-mSC[b]	**16.8***	**16.8***	**0.21***	**5.5**	**5.5**
12	PANI/CNT[b]	38				
22	CNT/MnO_2[a]		25.4			3.52
23	CNT/CNF[a]	86.8		6.3	9.8	
25	CNT/OMC[b]	39.7		1.91	1.77	
26	CNT/MnO_2[b]	3.01		0.015		1.73
27	CNT[b]	8.66	32.09	0.029		
28	Graphene[b]	1.7			0.17	
29	Graphene[b]	0.726		0.01		
30	ZnO nanowires[a]	2.4			0.027	
31	Pen ink[b]	26.4		1.008	2.7	
46	PEDOT/CNT[a]	73	179	0.47		1.4
47	CNT and Ti fibers[b]	0.6		0.024	0.15	
48	ZnO nanowires/graphene[a]	2		0.025		
49	PANI/stainless steel[b]	41			0.95	
50	Carbon/MnO_2[b]		2.5			0.22
52	PANI/graphene[b]	66.6				
55	CNT/graphene[b]	0.98				

[*] Specific capacitance of total cell (C_{tA}).

[a] Data obtained from CV tests.

[b] Data obtained from GCD tests.

Journal of Materials Chemistry A Accepted Manuscript

This journal is © The Royal Society of Chemistry [year]

Acknowledgments

This work is funded by the National Natural Science Foundation of China (no. 21325417 and no. 51173162), Huawei Innovation Research Program, Fundamental Research Funds for the Central Universities (no. 2013XZZX003), and Zhejiang Provincial Natural Science Foundation of China (no. R4110175).

Notes and references

[a] *MOE Key Laboratory of Macromolecular Synthesis and Functionalization, Department of Polymer Science and Engineering, Zhejiang University, 38 Zheda Road, Hangzhou, P. R. China. E-mail: chaogao@zju.edu.cn, cgao18@163.com.*

† Electronic Supplementary Information (ESI) available: [Calculation, Mechanical properties, Additional SEM photos, Additional electrochemical plots and tables]. See DOI: 10.1039/b000000x/

1 J. R. Miller, P. Simon, *Science*, 2008, **321**, 651.
2 P. Simon, Y. Gogotsi, *Nat. Mater.,* 2008, **7**, 845
3 M. Kaempgen, C. K. Chan, J. Ma, Y. Cui, G. Gruner, *Nano Lett.,* 2009, **9**, 1872.
4 X. Zhao, C. M. Hayner, M. C. Kung, H. H. Kung, *ACS Nan*o, 2011, **5**, 8739.
5 Y. Xu, Z. Lin, X. Huang, Y. Liu, Y. Huang, X. Duan, *ACS Nano*,2013, **7**, 4042.
6 J. Luo, H. D. Jang, J. Huang, *ACS Nano,* 2013, **7**, 1464.
7 Y. Fang, B. Luo, Y. Jia, X. Li, B. Wang, Q. Song, F. Kang, L. Zhi, *Adv.Mater.*,2012, **24**, 6348.
8 C. Yuan, L. Yang, L. Hou, J. Li, Y. Sun, X. Zhang, L. Shen, X. Lu, S. Xiong, X. W. Lou, *Adv. Funct. Mater.,* 2012, **22**, 2560.
9 L. Peng, X. Peng, B. Liu, C. Wu, Y. Xie, G. Yu, *Nano Lett.,* 2013, **13**, 2151.
10 Z. Wu, D. Wang, W. Ren, J. Zhao, G. Zhou, F. Li, H. Cheng, *Adv. Funct. Mater.,* 2010, **20**, 3595.
11 J. Yan, Z. Fan, W. Sun, G. Ning, T. Wei, Q. Zhang, R. Zhang, L. Zhi, F. Wei, *Adv. Funct. Mater.,* 2012, **22**, 2632.
12 K. Wang, Q. Meng, Y. Zhang, Z. Wei, M. Miao, *Adv. Mater.,* 2013, **25**, 1494.
13 Y. Zhao, J. Liu, Y. Hu, H. Cheng, C. Hu, C. Jiang, L. Jiang, A. Cao, L. Qu, *Adv. Mater.,* 2013, **25**, 591.
14 H. Cong, X. Ren, P. Wang, S. Yu, *Enery. Environ. Sci.,* 2013, **6**, 1185.
15 Z. Wu, W. Ren, D. Wang, F. Li, B. Liu, H. Cheng, *ACS Nano,* 2010, **4**, 5835.
16 J. Zhang, J. Jiang, H. Li, X. S. Zhao, *Enery. Environ. Sci.,* 2011, **4**, 4009.
17 Z. Fan, J. Yan, T. Wei, L. Zhi, G. Ning, T. Li, F. Wei, *Adv. Funct. Mater.,* 2011, **21**, 2366.
18 A. Sumboja, C. Y. Foo, X. Wang, P. S. Lee, *Adv. Mater.,* 2013, **25**, 2809.
19 H. Gao, F. Xiao, C. B. Ching, H. Duan, *ACS Appl. Mater. Interfaces,* 2012, **4**, 7020.
20 Y. Jin, H. Chen, M. Chen, N. Liu, Q. Li, *ACS Appl. Mater. Interfaces,* 2013, **5**, 3408.
21 X. Lu, M. Yu, G. Wang, T. Zhai, S. Xie, Y. Ling, Y. Tong, Y. Li, *Adv. Mater.,* 2013, **25**, 267.
22 C. Choi, J. A. Lee, A. Y. Choi, Y. T. Kim, X. Lepró, M. D. Lima, R. H. Baughman, S. J. Kim, *Adv. Mater.,* 2013, DOI: 10. 1002/ adma. 201304736.
23 V. T. Le, H. Kim. A. Ghosh, J. Kim, J. Chang, Q. A. Vu, D. T. Pham, J. Lee, S. Kim, Y. H. Lee, *ACS Nano,* 2013, **7**, 5940.
24 Y. Cheng, S. Lu, H. Zhang, C. V. Varanasi, J. Liu, *Nano Lett.,* 2012, **12**, 4206.
25 J. Ren, W. Bai, G. Guan, Y. Zhang, H. Peng, *Adv. Mater.,* 2013, **25**, 5965.
26 J. Ren, L. Li, C. Chen, X. Chen, Z. Cai, L. Qiu, Y. Wang, X. Zhu, H. Peng, *Adv. Mater.,* 2013, **25**, 1155.
27 X. Chen, L. Qiu, J. Ren, G. Guan, H. Lin, Z. Zhang, P. Chen, Y. Wang, H. Peng, *Adv. Mater.,* 2013, **25**, 6436.
28 Y. Meng, Y. Zhao, C. Hu, H. Cheng, Y. Hu, Z. Zhang, G. Shi, L. Qu, *Adv. Mater.,* 2013, **25**, 2326.
29 Y. Li, K. Sheng, W. Yuan, G. Shi, *Chem. Commun.,* 2013, **49**, 291.
30 J. Bae, M. K. Song, Y. J. Park, J. M. Kim, M. Liu, Z. L. Wang, *Angew. Chem. Int. Ed.,* 2011, **50**, 1683.
31 Y. Fu, X. Cai, H. Wu, Z. Lv, S. Hou, M. Peng, X. Yu, D. Zou, *Adv. Mater.,* 2012, **24**, 5713.
32 Z. Xu, C. Gao, *ACS Nano,* 2011, **5**, 2908.
33 Z. Xu, C. Gao, *Nat Commun,* 2011, **2**, 571.
34 Z. Xu, H. Sun, X. Zhao, C. Gao, *Adv. Mater.,* 2013, **25**, 188.
35 Z. Xu, Y. Zhang, P. Li, C. Gao, *ACS Nano,* 2012, **6**, 7103.
36 X. Hu, Z. Xu, C. Gao, *Sci. Rep.,* 2013, **2**, 767.
37 L. Kou, C. Gao, *Nanoscale,* 2013, **5**, 4370.
38 Z. Xu, Z. Liu, H. Sun, C. Gao, *Adv. Mater.,* 2013, **25**, 3249.
39 S. Pei, J. Zhao, J. Du, W. Ren, H. Cheng, *Carbon,* 2010, **48**, 4466.
40 S. Chen, J. Zhu, X. Wang, *ACS Nano,* 2010, **4**, 6212.
41 J. Yan, Z. Fan, T. Wei, W. Qian, M. Zhang, F. Wei, *Carbon, 2010*, **48**, 3825.
42 Y. Wang, S. F. Yu, C. Y. Sun, T. J. Zhu, H. Y. Yang, *J. Mater. Chem.,* 2012, **22**, 17584.
43 I. K. Moon, J. Lee, R. S. Ruoff, H. Lee, *Nat Commun,* 2010, **1**, 73.
44 H. Sun, Z. Xu, C. Gao, *Adv. Mater.,* 2013, **25**, 2554.
45 C. Meng, C. Liu, L. Chen, C. Hu, S. Fan, *Nano Lett.,* 2010, **10**, 4025.
46 J. A. Lee, M. K. Shin, S. H. Kim, H. U. Cho, G. M Spinks, G. G. Wallace, M. D. Lima, X. Lepró, M. E. Kozlov, R. H. Baughman, S. J. Kim, *Nat Commun,* 2013, **4**, 1970.
47 T. Chen, L. Qiu, Z. Yang, Z. Cai, J. Ren, H. Li, H. Lin, X. Sun, H. Peng, *Angew. Chem. Int. Ed.,* 2012, **41**, 11977.
48 J. Bae, Y.J Park, M. Lee, S. N. Cha, Y.J. Choi, C. S. Lee, J. M. Kim, Z. L. Wang, *Adv. Mater.,* 2011, **23**, 3446.
49 Y. Fu, H. Wu, S. Ye, X. Cai, X. Yu, S. Hou, H. Kafafy, D. Zou, *Energy Environ. Sci.,* 2013, **6**, 805.
50 X. Xiao, T. Li, P. Yang, Y. Gao, H. Jin, W. Ni, W. Zhan, X. Zhang, Y. Cao, J. Zhong, L. Gong, W. Yen, W. Mai, J. Chen, K. Huo, Y. Chueh, Z. L. Wang, J. Zhou, *ACS Nano,* 2012, **6**, 9200.
51 W. G. Pell, B. E. Conway, *J. Power. Sources,* 2004, **136**, 334.
52 T. Huang, B. Zheng, L. Kou, K. Gopalsamy, Z. Xu, C. Gao, Y. Meng, Z. Wei, *RSC. Adv.,* 2013, **3**, 23957.
53 C. Gao, C. D. Vo, Y. Z. Jin, W. Li, S. P. Armes, *Macromolecue*s, 2005, **38**, 8634.
54 B. Zheng, C. Gao, *Polymer Bulletin,* 2013, **10**, 171.
55 H. Cheng, Z. Dong, C. Hu, Y. Zhao, Y. Hu, L. Qu, N. Chen, L. Dai, *Nanoscale,* 2013, **5**, 3428.
56 F. Meng, J. Zhao, Y. Ye, X. Zhang, S. Li, J. Jia, Z. Zhang, Q. Li, *J. Mater. Chem.,* 2012, **22**, 1627.
57 X. Zhao, Z. Xu, B. Zheng, C. Gao, *Sci. Rep.,* 2013, **3**, 3164.
58 Y. Shang, Y. Li, X. He, S. Du, L. Zhang, E. Shi, S. Wu, Z. Li, J. Wei, *ACS Nano*, 2013, **7**, 1446.
59 L. Bao, X Li, *Adv. Mater.,* 2012, **24**, 3246.
60 V. L. Pushparaj, M. M. Shaijumon, A. Kumar, S. Murugesan, L. Ci, R. Vajtai, R. J. Linhardt, O. Nalamasu, P. M. Ajayan, PNAS, 2007, **104**, 13674.
61 Z. Xu, C. Gao, *Acc. Chem. Res.*, DOI:10.1021/ar4002813.
62 L. Kou, T. Q. Huang, B. N. Zheng, Y. Han, X. L. Zhao, K. Gopalsamy, C. Gao, *Nat. Commun.* 2014, **5**, 3754.

Journal of Materials Chemistry A Accepted Manuscript